Planar Light Concentration in Micro-Si Solar Cells Enabled by a Metallic Grating−Photonic Crystal Architecture

Liu Liu,[†] Greg D. Barber,[‡,§] Mikhail V. Shuba,[⊥,‖] Yu Yuwen,[†] Akhlesh Lakhtakia,[⊥] Thomas E. Mallouk,[#] and Theresa S. Mayer*,[†]

[†]Department of Electrical Engineering, [‡]Penn State Institutes of Energy and the Environment, [§]Department of Chemistry, [⊥]Department of Engineering Science and Mechanics, and [#]Departments of Chemistry, Biochemistry and Molecular Biology, and Physics, Pennsylvania State University, University Park, Pennsylvania 16802, United States
[‖]Institute for Nuclear Problems, Belarus State University, Bobruiskaya Street 11, Minsk 220030, Belarus

Ⓢ Supporting Information

ABSTRACT: A one-dimensional photonic crystal (1D PC) on top of a metal grating can efficiently couple incoming broadband, unpolarized light into multiple guided-wave modes (surface-plasmon-polariton waves and waveguide modes) with relatively long propagation lengths. These properties make this plasmonic architecture potentially attractive for solar concentration over length scales of tens to hundreds of micrometers. For proof-of-concept purposes, we have experimentally demonstrated a solar concentration device based on this plasmonic approach. The fabricated plasmonic concentrators were constructed as 1D-PC-loaded 1D metallic gratings, and microsolar cells were attached to the concentrators to test their performance. We found the plasmonic concentrators can have optical transfer efficiency of 24% at a concentration factor around 2×. In addition, light collection by the plasmonic concentrators was found to be insensitive to the angle of incidence of the light. Although the plasmonic concentrator structures realized in this study have modest efficiencies compared to conventional concentrator devices, the results allowed us to validate theoretical predictions of long propagation lengths and ultimately may help in the design of structures for improved performance. Our plasmonic-concentrator approach opens up new engineering opportunities for researchers to implement well-developed plasmonic theory into the design of broadband solar concentrating devices.

**KEYWORDS:** light concentrator, solar energy, surface-plasmon-polariton wave, waveguide modes
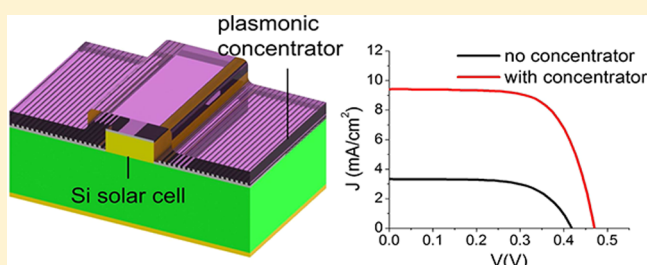
Plasmonic quasiparticles such as localized surface plasmons and surface-plasmon-polaritons (SPPs) have been of interest for decades because of their significance for field confinement and absorption enhancement of light.[1,2] Recent research has yielded many successful examples of wide-field-of-view plasmonic light absorbers in broad spectral regimes.[3−5] Their high efficiency and customized design have led to the incorporation of plasmonic light absorbers in the active regions of thin-film solar cells.[6] For example, integration of metallic nanoparticles[7−9] and gratings[10−12] has been reported to enhance the performance of thin-film solar cells by increasing light absorption in the active region of the cells. However, high ohmic loss in the metals used in these plasmonic structures causes dissipation of light and limits their effectiveness in delivering high-efficiency photovoltaic devices.[2]

We have recently reported a new strategy for broadband plasmonic absorption with low dissipation based on the excitation of multiple guided-wave modes (i.e., SPP waves as well as waveguide modes).[13,14] The absorber was constructed as a one-dimensional (1D) photonic crystal (PC) made of lossless isotropic dielectric materials, which was placed on top of either a 1D[13] or a 2D[14] gold grating. Incoming unpolarized light was

efficiently coupled into the guided-wave modes of both types of linear polarization states over a broad range of incident directions. Both the SPP waves and the waveguide modes guide light along the direction of the interface of the PC and the metal, but their physics are different. An SPP wave is bound to the planar interface of a metal and a dielectric material, whether homogeneous or not, in the direction normal to the interface, and its field profile is independent of the thickness of the dielectric material after it exceeds a threshold value.[1,15,16] In contrast, the field profile of a waveguide mode depends crucially on the thickness of the dielectric material.[17,18] In previous studies,[13,14] we have experimentally validated the theoretical predictions of electric-field concentration in the PC and low attenuation of the guided-wave modes (the propagation length of the guided-wave modes can be as long as millimeters).[15] The ability of these plasmonic architectures to collect light efficiently over broad spectral regimes and transport it over macroscopic distances raises the question of
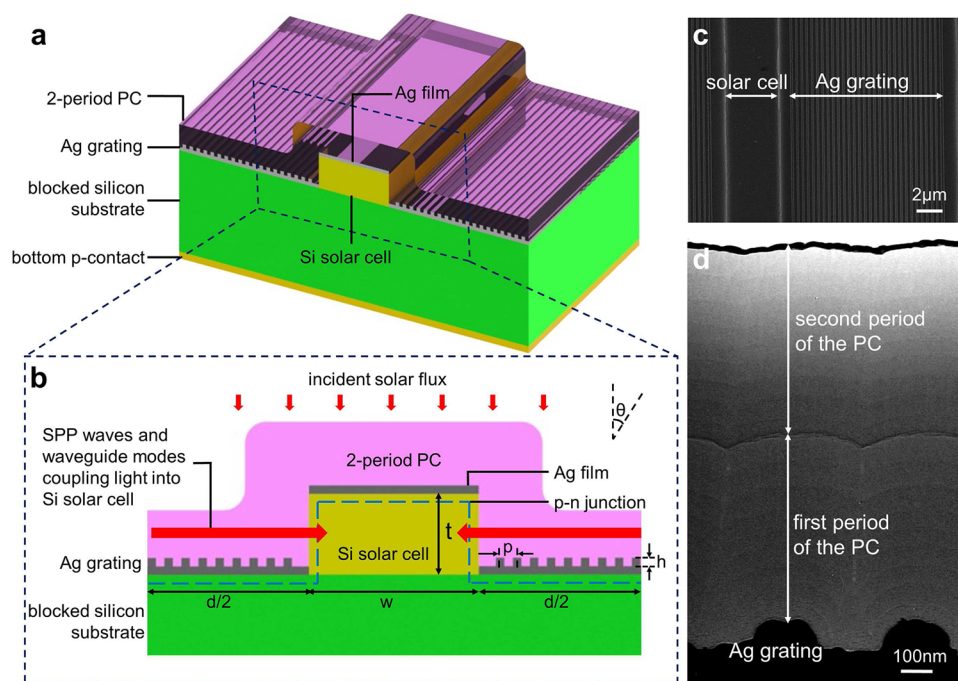
Figure 1. (a) Schematic of a device consisting of a Si solar cell attached between two plasmonic concentrators supported on a thick Si substrate with bottom p-contact. The n-contact surrounds the device active area and is not shown here. (b) Cross-sectional schematic of a device in arrays labeled S1 and S2 with geometric parameters listed and light-coupling mechanisms illustrated. The Si solar cell is constructed as a radial p−n junction with the junction indicated by the dashed blue lines. (c) Top-view SEM image of the device before the deposition of the PC, showing the arrangement of the solar cell and the 1D Ag grating at the bottom of a plasmonic concentrator. (d) Cross-sectional TEM image showing the structure of a plasmonic concentrator constructed as a two-period-thick PC on a 1D Ag grating. Each period of the PC comprised the same nine-layer stack of silicon oxynitrides.

whether such structures can be useful in solar concentration applications.[19] Because broadband, efficient, and stationary (tracker-free) solar-concentration devices are highly desired for roof-top solar harvesting applications,[20−22] it is worthwhile to address this question and explore the potential of this plasmonic architecture for planar light concentration.

In this paper, we demonstrate at the proof-of-concept level the ability of a 1D-PC-loaded metallic 1D grating to concentrate light in a planar microconcentrator architecture. Although the structures used in this study have modest efficiencies compared to conventional planar concentrator devices,[22−25] the results allow us to validate the theoretically predicted long propagation length of light in PC-coupled plasmonic structures and could help improve our understanding of the plasmonic light-concentration effects. The plasmonic-concentrator approach thus opens up new engineering opportunities for researchers to implement well-developed plasmonic theory into the design of broadband solar concentrating devices.

■ RESULTS AND DISCUSSION

Device Fabrication. As a proof-of-concept, we fabricated test structures on monolithic silicon (Si) wafers, as shown in Figure 1. Although they are simple to fabricate, the solar cells have low efficiency because of the high doping density and the radial p−n junction architecture used. Nevertheless, the enhancement factors we measured allowed us to assess the optical characteristics of the planar plasmonic solar concentrators.

Two test structures (labeled S1 and S2) were fabricated as 1D arrays of equally spaced solar cells. Each array was 5 mm ×

5 mm in area, and every solar cell in both arrays had a length L = 5 mm, width w = 4.5 ± 0.3 μm, and thickness t = 1.3 ± 0.2 μm. The Si solar cells in each structure were constructed in radial-junction configuration shown in Figure 1b. The n-type emitter was formed by thermal diffusion with a peak doping density of 1×10^{21} cm^{-3} at the surface of the arrays, and the p-type base with a doping density of 5×10^{18} cm^{-3}. After patterning the solar cells, a p-contact (Figure 1a) was formed at the bottom of the substrate and an n-contact (not shown) was fabricated around each array. An optically thick (150 nm) silver (Ag) film was deposited on the top of the solar cells to block normally incident light so that (1) light absorption in each cell could be attributed solely to light concentration and (2) the thick Si substrate would not generate photocurrent to complicate the situation. The fabrication techniques are described in detail in the Materials and Methods section.

Schematics of the devices in arrays S1 and S2 are presented in Figure 1a,b. In these arrays, a plasmonic concentrator of fixed length d and grating period p = 400 nm was interposed between every pair of adjacent solar cells so that the center-to-center distance between adjacent solar cells was $d + w$. Each plasmonic concentrator consisted of a 1D Ag grating and a two-period PC with each period comprising nine silicon-oxynitride layers of different compositions (Figure 1c,d). The grating had a height h = 86 nm and a trough width of 0.6p. The lengths of the concentrators were d = 13.77 μm in S1 and d = 10.25 μm in S2. The refractive indices of the silicon-oxynitride layers and Ag are provided in the Supporting Information as functions of the free-space wavelength λ_0 (Figure S1). It is worth noting here that the choice of materials for the PC is flexible as long as the chosen materials are virtually nondissipative in the solar spectral regime.
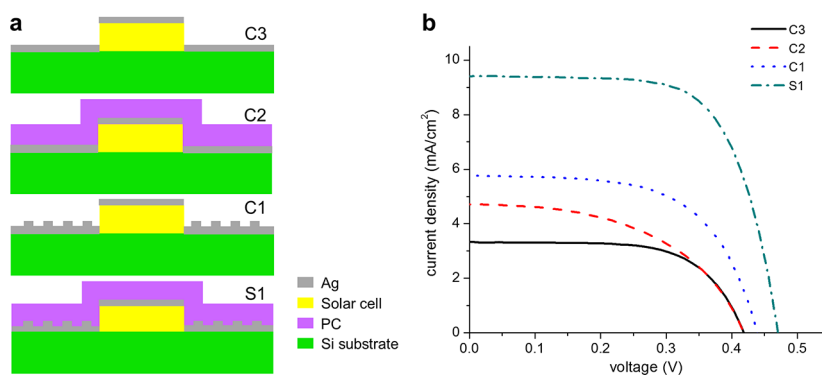
Figure 2. (a) Schematics of the devices in array S1 and the control samples. (b) Measured $J-V$ curves of these devices.
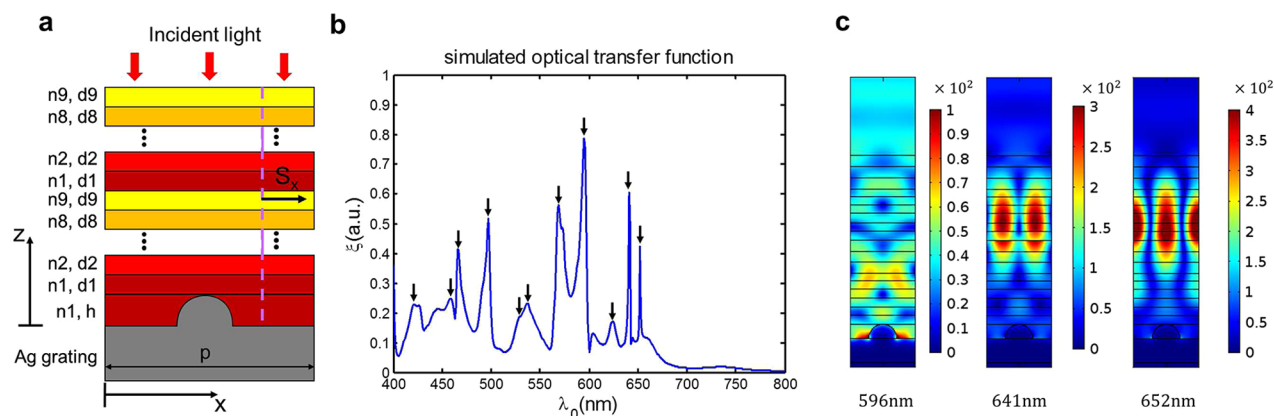
Figure 3. (a) Schematic of one unit cell of the plasmonic concentrator. The simulated optical transfer function ξ was calculated as the normalized bidirectional optical power flux crossing the plane $x = (3/4)p$ shown by the purple dashed line. (b) Spectrum of ξ with peaks marked with black arrows. (c) Spatial distribution of the magnitude (in V m^{-1}) of the electric field at $\lambda_0 \in \{596, 641, 652\}$ nm, in the unit cell of the planar concentrator when the incident light is unpolarized and $S_{\text{inc}} = 1$ W m^{-2}.

Effectiveness of Plasmonic Concentrator. In order to validate the light concentration effect in the plasmonic-concentrator approach, we also fabricated three control structures (labeled C1 to C3) as 5 mm × 5 mm arrays of equally spaced solar cells. The control structures were constructed with the same w and d as S1 but did not have the complete plasmonic concentrators, as shown schematically in Figure 2a. Every concentrator in C1 lacked the two-period PC. In C2, every planar concentrator was replaced by a two-period PC on top of a 150-nm-thick Ag layer. Finally, C3 was the same as C2, except that the PCs were absent. The values of t were close enough in array S1 and the control samples: 1.4 μm for S1 and C1 and 1.1 μm for C2 and C3.

We evaluated the effectiveness of the plasmonic concentrator by comparing the short-circuit current density J_{sc} and efficiency η of the solar cells in arrays S1, C1, C2, and C3. Figure 2b shows the current density $J = I/A_0$ (where I is the current and $A_0 = L^2w/(w + d)$ is the combined isolation area of all solar cells in the array) as a function of the applied voltage V for these four arrays. Measurements were carried out for normal illumination using a standard solar simulator (Oriel Sol3A Class AAA, Newport, Irvine, CA, USA) with the irradiance set to one sun using a calibrated NREL-certified reference cell.

Blocked from receiving direct normal illumination due to the 150-nm-thick Ag film at the top, C3 could receive only light that has been diffracted by the periodically arranged solar cells in the array. Indeed, diffraction of light by C3 was experimentally evident from the observed diffraction pattern

generated when C3 was placed under normal light illumination. In addition, the edges of the solar cells facilitate light scattering that could also contribute to the absorption of photons. Therefore, the $J-V$ curve of C3 shows only these two contributions and has the lowest values of J_{sc} (3.32 mA cm^{-2}) and η (0.88%). The control structure C2 had slightly higher efficiency than C3 because of the incorporation of the two-period PC. As the refractive indices of all layers in the PC lay between those of air and crystalline Si, the PC functioned as an imperfect antireflection coating that enhanced the efficiency η from 0.88% for C3 to 0.99% for C2. C1 differed from C3 only in having the 150-nm-thick Ag film between adjacent solar cells replaced by a Ag grating. These gratings can couple p-polarized (magnetic field parallel to the grating lines) incident light into SPP waves[1,15] that travel toward the sidewalls of the solar cells. The additional light entering the solar cells enhanced η from 0.88% for C3 to 1.38% for C1, the enhancement factor being 1.57.

Finally, S1 had both the Ag gratings of C1 and the two-period PC of C2; that is, S1 had the complete plasmonic concentrator between every pair of adjacent solar cells. Multiple SPP waves[13,14] and waveguide modes[14,26] were excited to steer even more light toward the sidewalls of the solar cells in S1. Accordingly, the efficiency of S1 rose to 2.84%—about 3.2 times the efficiency of C3—validating the light-concentration effect in this plasmonic architecture.

The efficiencies of array S1 and the control structures are strongly correlated to the respective values of J_{sc}. Thus, J_{sc} of S1

was the highest at 9.28 mA cm^{-2}, while that of C3 was the lowest at 3.32 mA cm^{-2}, the ratio being 2.98 in favor of S1. We extracted values of the fill factor (FF)[27] from the J–V curves in Figure 2b. Structures S1, C1, and C3 had quite similar fill factors (63.5 ± 3.5%), while that of C2 was significantly lower (51%). Nevertheless, the progression of the values of J_{sc}, which is proportional to the absorption of photons in the solar cells, clearly demonstrates the efficacy of the plasmonic concentrator.

Simulation of Light Transport in Plasmonic Concentrator. We theoretically evaluated the light-concentration effect of the plasmonic concentrator alone by simulating light transport therein using COMSOL Multiphysics software, after assuming that unpolarized light is normally incident on the concentrator with infinite extent in the transverse plane. The cross-section of one unit cell of the concentrator is shown in Figure 3a. The grating was assumed to have semicircular features consistent with the TEM image shown in Figure 1d. The planar two-period PC of total thickness $D = 2(d_1 + d_2 + ... + d_N)$ was separated from the grating by a spacer of maximum thickness h (Figure 3a).

With S_{inc} denoting the monochromatic incident time-averaged power density, the x-directed component $S_x(x,z,\lambda_0)$ of the monochromatic time-averaged Poynting vector $\mathbf{S}(x,z,\lambda_0)$ was computed everywhere in the concentrator for $\lambda_0 \in [400, 800]$ nm. Then, we computed the normalized bidirectional optical power flux:

$$\xi(\lambda_0) = \frac{1}{pS_{inc}} \int_0^{h+D} |S_x(3p/4, z, \lambda_0)| \, dz \qquad (1)$$

crossing the plane $x = (3/4)p$ (shown as the purple dashed line in Figure 3a) as a measure of the efficiency of the redirection of the normally incident optical energy toward the sidewalls of the solar cells. The spectrum of this simulated optical transfer function ξ is useful for identifying resonances.

The spectrum of $\xi(\lambda_0)$ is presented in Figure 3b with 11 peaks marked with black arrows. These peaks indicate that the incident light is highly coupled at multiple resonances in the spectral range 400 to 670 nm. We found that 10 of the 11 peaks indicate the excitation of guided-wave modes of either the p-polarization state or the s-polarization state (electric field parallel to the grating lines). The peak at $\lambda_0 = 596$ nm is due to a p-polarized SPP wave[13,14] guided by the metal/PC interface. Likewise, the peaks at 528 and 624 nm are due to s-polarized SPP waves,[13,14] with the one at the shorter wavelength less localized to the metal/PC interface than the one at the longer wavelength. The peaks at 467, 569, and 641 nm are due to the p-polarized modes[14] of a planar metal/PC/air waveguide. The peaks at 458 and 652 nm are due to the s-polarized modes[14] of the same waveguide. Finally, each of the peaks at 497 and 530 nm is due to closely spaced p- and s-polarized modes of the same waveguide. We were unable to find a reason for the peak at 421 nm in Figure 3b.

The intensity profile of light inside the plasmonic concentrator is also crucial for its performance. The electric field of a conventional SPP wave guided by the interface of a metal and a homogeneous dielectric material is concentrated near the interface, resulting in high dissipation in the metal and a short propagation length.[1] In addition, as the thin-film solar cells attached to the concentrators usually have their lowest collection efficiency in the heavily doped regions at the top and the bottom,[12] it is desirable to have light either concentrated at

the center of the planar concentrator or distributed evenly along the height of the solar cells for better performance.

The simulated spatial profiles of the magnitude of the electric field inside the unit cell of the plasmonic concentrator are plotted in Figure 3c for three resonance wavelengths: 596, 641, and 652 nm. Each of these peaks is due to the excitation of a different kind of guided-wave mode. The electric field has high magnitudes in the central region of the nondissipative PC in all three cases. In the other cases, the electric field is distributed evenly along the z axis.

Determination of Optical Transfer Efficiency (η_{opt}) of Plasmonic Concentrator. In order to describe the efficiency of the plasmonic concentrators to couple incident light into guided-wave modes, we defined the wavelength-dependent optical transfer efficiency ($\eta_{opt}(\lambda_0)$) as the ratio of the measured external quantum efficiency ($EQE_{array}(\lambda_0)$) of the arrays and the simulated average external quantum efficiency ($EQE_{cell}(\lambda_0)$) of the solar cells. This normalization by the latter quantity eliminates the effect of the performance of the solar cells in the spectrum of $EQE_{array}(\lambda_0)$ and reveals the optical transfer efficiency of the plasmonic concentrator alone. The same characterization was also done for the control structure C2 in which a 150-nm-thick film of Ag was present instead of the Ag grating.

For the experimental determination of $EQE_{array}(\lambda_0)$, the arrays were illuminated normally by monochromatic light whose wavelength λ_0 was swept from 400 to 800 nm. Both the power density (S_{inc}) of the light source and the short-circuit current density (J_{sc}) of the arrays were measured as functions of λ_0 to determine

$$EQE_{array}(\lambda_0) = \frac{2\pi\hbar c}{e\lambda_0} \frac{J_{sc}(\lambda_0)}{S_{inc}(\lambda_0)} \qquad (2)$$

where $\hbar = 1.054 \times 10^{-34}$ J s^{-1} is the normalized Planck constant, $c = 3 \times 10^8$ m s^{-1} is the speed of light in free space, and $e = 1.6 \times 10^{-19}$ C is the elementary charge. Accordingly,

$$\eta_{opt}(\lambda_0) = \frac{EQE_{array}(\lambda_0)}{EQE_{cell}(\lambda_0)} = \frac{2\pi\hbar c}{e\lambda_0} \frac{J_{sc}(\lambda_0)}{S_{inc}(\lambda_0) \, EQE_{cell}(\lambda_0)} \qquad (3)$$

We determined $EQE_{cell}(\lambda_0)$ by simulating a 4.5-μm-thick crystalline-silicon solar cell of infinite transverse extent using wxAMPS software.[28] The thickness of this solar cell was set equal to the width (w) of the solar cells in the arrays to mimic light entering through the sidewalls of the cells. The spectrum of EQE_{cell} is plotted in the inset of Figure 4, other details of the simulation being provided in the Supporting Information.

Due to fabrication imperfections, the actual external quantum efficiencies of the solar cells in the arrays should not exceed EQE_{cell} values yielded by the simulation; thus, the spectra of $\eta_{opt}(\lambda_0)$ of the arrays S1, S2, and C2 presented in Figure 4 represent conservative estimates. In most of the [400, 800] nm spectral regime, η_{opt} hovers around 15%, with the highest value of 24% at $\lambda_0 = 645$ nm for S2 and 21% at $\lambda_0 = 653$ nm for S1. The optical transfer efficiency of the planar concentrators in S1 is generally lower than that in S2. This is because the longer Ag gratings between two adjacent solar cells in S1 lead to greater optical attenuation in the planar concentrators of S1, in comparison to S2. Corroboration of that conclusion also comes from the decrease of η_{opt} for $\lambda_0 \lesssim 500$ nm due to stronger absorption in Ag at shorter wavelengths.[29]
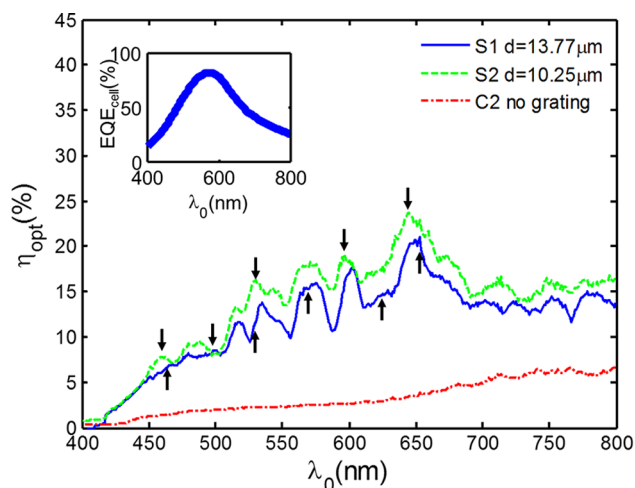
Figure 4. Spectra of η_{opt} of arrays S1, S2, and C2 as functions of λ_0. Inset: Simulated spectrum of EQE_{cell}.

Figure 4 also presents the very low optical transfer efficiency of the two-period PC on top of a 150-nm-thick Ag layer in C2, highlighting the significant role of the Ag grating in the plasmonic concentrators. The roughly tripling of η_{opt} by use of the metal grating in comparison to the planar metal layer is due to the excitation of guided-wave modes at multiple wavelengths by the former. Evidence for the excitation of these modes in the plasmonic concentrators in the arrays is provided by the excellent agreement of the occurrences of the peaks in Figure 4 for S1 and S2 with the occurrences of the peaks in Figure 3b. As discussed for the simulated spectrum in Figure 3b, the peaks arise from the excitation of multiple SPP waves[13,14] and waveguide modes[14] in every plasmonic concentrator between adjacent solar cells.

If the corrugations of the grating are planarized, not only will these peaks vanish but also $S_x \equiv 0$, which implies that $\xi \equiv 0$. No peaks are evident in the spectrum of η_{opt} in Figure 4 for C2. The nonzero (but small) values of η_{opt} at shorter wavelengths for C2 are very likely due to surface imperfections of the Ag layer. The somewhat larger values of η_{opt} at longer wavelengths for C2 are due to the visually observable optical diffraction by the exposed sidewalls of the periodically arranged solar cells in that array.

The same diffraction is responsible for the excess of η_{opt} for S1 and S2 in Figure 4 over ξ in Figure 3b when $\lambda_0 \lesssim 700$ nm, no solar cell being present in the simulation for Figure 3b. The diffraction by the periodic array of solar cells even couples into guided-wave modes in the plasmonic concentrators, as is evident from the peaks of η_{opt} for S1 and S2 in Figure 4.

Concentration Factor of Plasmonic Concentrator. The performance of a solar concentrator is often evaluated in terms of the concentration factor F,[30] defined as the ratio of the efficiency of a solar cell used with the concentrator to the efficiency of the same solar cell used without the concentrator. The experimentally measured concentration factor of a particular concentrator often depends strongly on the geometry and arrangement of the concentrator and the attached solar cells.

In our experiments, as the solar cells were blocked from the top by the 150-nm-thick Ag layer, their efficiency was close to zero when used without the plasmonic concentrators. Therefore, the concentration factor would be artificially exaggerated if determined solely by measuring the efficiencies of the solar cells

with and without the concentrator. Therefore, we simulated the efficiency η_{cell} of a solar cell alone by using wxAMPs software, just as we had determined $EQE_{cell}(\lambda_0)$. Assuming that the actual solar cells performed as well as the simulated ones, we determined the semiexperimental estimate $\tilde{F}$ of F as

$$\tilde{F} = 1 + \frac{\eta}{\eta_{cell}} \qquad (4)$$

The wxAMPS simulation[28] yielded η_{cell} = 3.06% for a crystalline-silicon solar cell of thickness $t = 1.3$ μm. The similar measured efficiency of Si solar cells of closely related structures justified the use of this value as a reasonable estimate of η_{cell}.[31] Substituting η_{cell} = 3.06% into eq 4, values of $\tilde{F}$ for arrays S1 and S2 are presented in Table 1, where $G = d/w$ is the geometric

Table 1. Semiexperimental Estimate $\tilde{F}$ of the Concentration Factor F in Relation to the Geometric Gain G for Arrays S1 and S2

array	S1	S2
G	3.2	2.6
$\tilde{F}$	1.97	1.76

gain. Optical-only simulations of the plasmonic concentrator with the similar 1D-grating configuration indicate that $F \approx 2.5$ should be possible for $G = 3.0$,[19] which is higher than the value of $\tilde{F}$. This difference is likely caused by the differences in the geometries of experimental arrays and the simulated planar concentrator:[19] for the simulations, the width w of the attached solar cells was taken to be very small (400 nm) due to the limit of computational power; therefore, the width d of the plasmonic concentrator was also small for the same values of G ($d = 400$ and 1200 nm for $G = 2$ and 3, respectively). In contrast, the fabricated structures presented in this paper have 10-fold larger values of d and w. As discussed for Figure 4, an increase in d reduces η_{opt} and therefore η, thereby making F smaller than theoretical predictions. Moreover, fabrication imperfections could also reduce the performance of the plasmonic concentrator. For example, the profile of the two-period PC close to the edge of a solar cell has significant distortion due to the limitations of plasma-enhanced chemical vapor deposition used to deposit the PC, as is evident from Figure 5. Unlike the simulated structures wherein the PC layers were assumed to uniformly fill the space between adjacent solar cells, the PC layers in the fabricated devices were thin near the edge of the cells and followed the surface topography around the cells. The distorted PC could guide light over the solar cells and/or increase light reflection at the interfaces of the PC and the solar cells, and thus decrease the light collection efficiency.

Angular Response of Plasmonic Concentrators. The performance of planar concentrators should remain constant even as the direction of incident light changes. The angular dependence of the performance of our planar plasmonic concentrator was investigated by mounting each of the arrays S1 and S2 on a rotatable sample stage and measuring their $J-V$ curve on the solar simulator for different incidence angles $\theta \in \{0°, \pm10°, \pm30°, \pm50°\}$ (Figure 1d). The estimated concentration factors $\tilde{F}$ determined thereafter using eq 4 are presented in Figure 6. To determine the values of η_{cell} under oblique incidence conditions, the measured power output of the solar cells was divided by $P_0 \cos\theta$, where P_0 is the power of the incident light at normal incidence. The inclusion of the factor $\cos\theta$ accounts for the reduction in photon flux from the
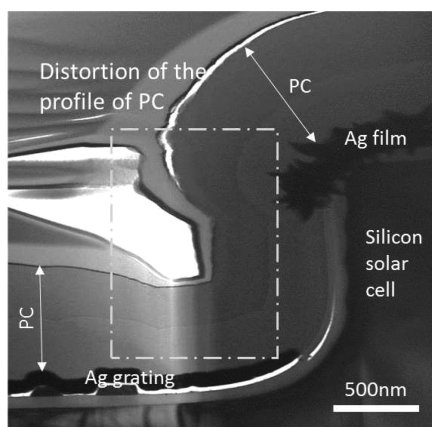
Figure 5. Cross-sectional TEM image of an array, showing the distortion of the two-period PC in the vicinity of a solar cell. There is no material in the white areas. The gray box highlights the distortion of the profile of the two-period PC.
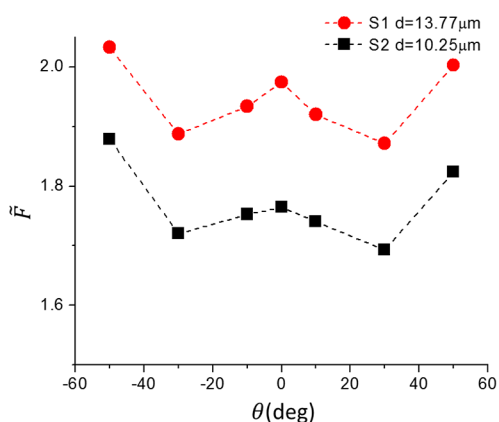
Figure 6. Semiexperimentally estimated concentration factors $\tilde{F}$ of arrays S1 and S2 for oblique incidence.

solar simulator when $\theta \neq 0$. From the figure, we conclude that $\tilde{F}$ of all three arrays are quite stable with respect to the incidence direction and may even be higher for quite oblique incidence than for normal incidence.

Previous experimental and theoretical results[14] indicate that numerous guided-wave modes exist in different portions of the $\lambda_0 \times \theta$ space. As the angle θ increases from $0°$, different modes will turn on and off so that peaks in a diagram of η_{opt} vs λ_0 will shift and change in magnitude. The excitation of several different guided-wave modes appears responsible for the stability of $\tilde{F}$ over a broad range of θ.

CONCLUSION

A one-dimensional photonic crystal on top of a metal grating can efficiently couple incoming broadband, unpolarized light into multiple guided-wave modes (surface-plasmon-polariton waves and waveguide modes) with low attenuation. These properties make this plasmonic architecture potentially attractive for solar concentration over length scales of tens to hundreds of micrometers. We have experimentally demonstrated this idea at the proof-of-concept level using a 1D-PC-loaded metallic grating to guide light into silicon microcells fabricated in the same plane. These results validate theoretical predictions of long propagation lengths for guided-wave modes in coupled plasmonic–photonic crystal architectures.

We found that solar cells attached to the plasmonic concentrators had a factor of 3 times higher photocurrent than cells that were not attached. From the simulated optical transfer function, we predicted the resonances of the plasmonic concentrators. The optical transfer efficiency spectra of experimentally fabricated plasmonic concentrators exhibited the predicted resonances. We observed broadband light concentration over the solar spectrum and found an optical transfer efficiency (η_{opt}) of 24%.

The highest concentration factors of the structures tested in this preliminary study were around 2×, but higher values should be possible by using different architectures for the arrays. Interestingly, the performance of plasmonic concentrators did not degrade when light was obliquely incident in a wide angular sector, indicating possible utility in stationary light-concentration applications.

MATERIALS AND METHODS

Fabrication of Silicon Solar Cell Array. A heavily doped p-type silicon wafer (0.01−0.02 Ω·cm, University Wafer, Boston, MA, USA) was used to fabricate the solar cells. A 200-nm-thick SiO_2 layer was first grown on the wafer with thermal oxidation (wet) at 1000 °C. Silicon solar-cell microarrays (with geometries described in the paper) were then patterned by optical lithography (MA/BA6, Suss Micro-Tec, Garching, Germany) and etched into silicon using a deep reactive ion etching (DRIE) system (Speeder 100Si, Alcatel Micro Machining Systems, Nashua, NH, USA). The sample was then cleaned with piranha solution. A 400-nm-thick SiO_2 layer was grown on the sample by thermal oxidation (wet) and then removed by a buffered oxide etch 10:1 (BOE 10:1, Avantor Puerformance Materials, Center Valley, PA, USA) to eliminate the damaged surface layer of the sample resulting from the DRIE process. A 200-nm-thick SiO_2 layer was then thermally grown on the sample to serve as a diffusion barrier for the following doping step. Square-shaped (6 × 6 mm²) diffusion windows were then opened on top of the microarrays by optical lithography, and the thermal SiO_2 layer inside each diffusion window was etched away by a 10:1 buffered oxide etch. Phosphorus was then diffused into silicon in the diffusion windows at 1000 °C for 10 min to form a radial junction on each microarray. Then 250-μm-wide square rings were patterned around the microarrays on the edge of the diffusion windows by optical lithography. The SiO_2 layer in the rings was etched away in BOE 10:1. Then, 10-nm-thick Ti and 100-nm-thick Au layers were consecutively deposited in the rings using e-beam deposition (Semicore E-Gun thermal evaporator, Semicore Equipment Inc., Livermore, CA, USA) and a lift-off process in 1165 developer (Shipley, Marlborough, MA, USA). Finally, SiO_2 on the backside of the wafer was removed in the BOE 10:1, and 10-nm-thick Pt and 150-nm-thick Au layers were consecutively deposited using the same evaporation equipment on the backside.

Fabrication of Plasmonic Concentrators. The plasmonic concentrators were fabricated in the trenches between adjacent solar cells after the microarrays had been fabricated. ZEP520 photoresist (Zeon, Tokyo) was spin-coated on top of the microarrays, and e-beam lithography (EBPG5200, Raith America Inc., Troy, NY, USA) was used to define the geometry of the 1D grating arrays in the trench centers. A 90-nm-thick titanium (Ti) layer was deposited on top of the sample by e-beam evaporation (Semicore E-Gun thermal evaporator, Semicore Equipment Inc.) followed by a lift-off process in

1165 developer (Shipley) to form a Ti grating in the trenches. A 150-nm-thin layer of Ag was then coated on top of the sample by e-beam deposition to cover the top of the silicon solar cells and the Ti grating. Finally, the two-period PC was coated on top of the structure by plasma-enhanced chemical vapor deposition on a cluster tool (Applied Materials, Santa Clara, CA, USA).

■ ASSOCIATED CONTENT

Ⓢ Supporting Information

The Supporting Information is available free of charge on the ACS Publications website at DOI: 10.1021/acsphotonics.5b00706.

> Spectra of the refractive indices of Ag and silicon oxynitrides of nine different compositions; parameters used for the simulation of silicon solar cells using wxAMPS software (PDF)

■ AUTHOR INFORMATION

Corresponding Author
*E-mail (T. S. Mayer): tsm2@psu.edu.

Notes
The authors declare no competing financial interest.

■ ACKNOWLEDGMENTS

■ REFERENCES

(1) Maier, S. A. *Plasmonics: Fundamentals and Applications*; Springer: Heidelberg, 2007.

(2) Maier, S. A.; Atwater, H. A. Plasmonics: Localization and guiding of electromagnetic energy in metal/dielectric structures. *J. Appl. Phys.* 2005, 98, 011101.

(3) Bossard, J. A.; Lin, L.; Yun, S.; Liu, L.; Werner, D. H.; Mayer, T. S. Near-ideal optical metamaterial absorbers with super-octave bandwidth. *ACS Nano* 2014, 8, 1517−1524.

(4) Aydin, K.; Ferry, V. E.; Briggs, R. M.; Atwater, H. A. Broadband polarizationindependent resonant light absorption using ultrathin plasmonic super absorbers. *Nat. Commun.* 2011, 2, 517.

(5) Wu, C.; Neuner, B.; Shvets, G.; John, J.; Milder, A.; Zollars, B.; Savoy, S. Large-area wide-angle spectrally selective plasmonic absorber. *Phys. Rev. B: Condens. Matter Mater. Phys.* 2011, 84, 075102.

(6) Atwater, H. A.; Polman, A. Plasmonics for improved photovoltaic devices. *Nat. Mater.* 2010, 9, 205−213.

(7) Nakayama, K.; Tanabe, K.; Atwater, H. A. Plasmonic nanoparticle enhanced light absorption in GaAs solar cells. *Appl. Phys. Lett.* 2008, 93, 121904.

(8) Pillai, S.; Catchpole, T. T.; Green, M. A. Surface plasmon enhanced silicon solar cells. *J. Appl. Phys.* 2007, 101 (9), 093105.

(9) Catchpole, K. R.; Polman, A. Plasmonic solar cells. *Opt. Express* 2008, 16, 21793−21800.

(10) Ferry, V. E.; Verschuuren, M. A.; Bongbo, B. T.; Verhagen, E.; Walters, R. J.; Schropp, R. E. I.; Atwater, H. A.; Polman, A. Light trapping in ultrathin plasmonic solar cells. *Opt. Express* 2010, 18, A237−A245.

(11) Munday, J. N.; Atwater, H. A. Large integrated absorption enhancement in plasmonic solar cells by combining metallic gratings and antireflection coatings. *Nano Lett.* 2011, 11 (6), 2195−2201.

(12) Deceglie, M. G.; Ferry, V. E.; Alivisatos, A. P.; Atwater, H. A. Design of nanostructured solar cells using coupled optical and electrical modeling. *Nano Lett.* 2012, 12 (6), 2894−2900.

(13) Hall, A. S.; Faryad, M.; Barber, G. D.; Liu, L.; Erten, S.; Mayer, T. S.; Lakhtakia, A.; Mallouk, T. E. Broadband light absorption with multiple surface plasmon polariton waves excited at the interface of a metallic grating and photonic crystal. *ACS Nano* 2013, 7, 4995−5007.

(14) Liu, L.; Faryad, M.; Hall, A. S.; Barber, G. D.; Erten, S.; Mallouk, T. E.; Lakhtakia, A.; Mayer, T. S. Experimental excitation of multiple surface-plasmon-polariton waves and waveguide modes in a one-dimensional photonic crystal atop a two-dimensional metal grating. *J. Nanophotonics* 2015, 9, 093593.

(15) Polo, J. A., Jr.; Mackay, T. G.; Lakhtakia, A. *Electromagnetic Surface Waves: A Modern Perspective*; Elsevier: Waltham, 2013.

(16) Faryad, M.; Lakhtakia, A. On surface plasmon-polariton waves guided by the interface of a metal and a rugate filter with a sinusoidal refractive-index profile. *J. Opt. Soc. Am. B* 2010, 27 (11), 2218−2223.

(17) Kapany, N. S.; Burke, J. J. *Optical Waveguides*; Academic Press: New York, 1972.

(18) Snyder, A. W.; Love, J. D. *Optical Waveguide Theory*; Chapman and Hall: New York, 1983.

(19) Solano, M. E.; Barber, G. D.; Lakhtakia, A.; Faryad, M.; Monk, P. B.; Mallouk, T. E. Buffer layer between a planar optical concentrator and a solar cell. *AIP Adv.* 2015, 5, 097150.

(20) Debije, M. G.; Verbunt, P. P. C. Thirty years of luminescent solar concentrator research: Solar energy for the built environment. *Adv. Energy Mater.* 2012, 2, 12−35.

(21) Currie, M. J.; Mapel, J. K.; Heidel, T. D.; Goffri, S.; Baldo, M. A. High-efficiency organic solar concentrators for photovoltaics. *Science* 2008, 321 (5886), 226−228.

(22) Yoon, J.; Li, L.; Semichaevsky, A. V.; Ryu, J. H.; Johnson, H. T.; Nuzzo, R. G.; Rogers, J. A. Flexible concentrator photovoltaics based on microscale silicon solar cells embedded in luminescent waveguides. *Nat. Commun.* 2011, 2, 343.

(23) Yoon, J.; Baca, A. J.; Park, S.-I.; Elvikis, P.; Geddes, J. B., III; Li, L.; Kim, R. H.; Xiao, J.; Wang, S.; Kim, T.-H.; Motala, M. J.; Ahn, B. Y.; Duoss, E. B.; Lewis, J. A.; Nuzzo, R. J.; Ferreira, P. M.; Huang, Y.; Rockett, A.; Rogers, J. A. Ultrathin silicon solar microcells for semitransparent, mechanically flexible and microconcentrator module designs. *Nat. Mater.* 2008, 7, 907−915.

(24) Lee, S.-M.; Biswas, R.; Li, W.; Kang, D.; Chang, L.; Yoon, J. Printable nanostructured silicon solar cells for high-performance, large-area flexible photovoltaics. *ACS Nano* 2014, 8, 10507−10516.

(25) Xu, Z.; Yao, Y.; Brueckner, E. P.; Li, L.; Jiang, J.; Nuzzo, R. G.; Liu, G. L. Black silicon solar thin-film microcells integrating top nanocone structures for broadband and omnidirectional light-trapping. *Nanotechnology* 2014, 25, 305301.

(26) Khaleque, T.; Magnusson, R. Light management through guided-mode resonances in thin-film silicon solar cells. *J. Nanophotonics* 2014, 8, 083995.

(27) Fonash, S. J. *Solar Cell Device Physics*, 2nd ed.; Elsevier: Burlington, VT, 2010.

(28) Liu, Y.; Sun, Y.; Rockett, A. A new simulation software of solar cells—wxAMPS. *Sol. Energy Mater. Sol. Cells* 2012, 98, 124−128.

(29) Rakić, A. D.; Djurisić, A. B.; Elazar, J. M.; Majewski, M. L. Optical properties of metallic films for vertical-cavity optoelectronic devices. *Appl. Opt.* 1998, 37, 5271−5283.

(30) Parida, B.; Iniyan, S.; Goic, R. A review of solar photovoltaic technologies. *Renewable Sustainable Energy Rev.* 2011, 15, 1625−1636.

(31) Yoon, H. P.; Yuwen, Y. A.; Kendrick, C. E.; Barber, G. D.; Podraza, J. J.; Redwing, J. M.; Mallouk, T. E.; Wronski, C. R.; Mayer, T. S. Enhanced conversion efficiencies for pillar array solar cells fabricated from crystalline silicon with short minority carrier diffusion lengths. *Appl. Phys. Lett.* 2010, 96 (21), 213503.